

WEAR AND MECHANICAL PROPERTIES OF SPARK PLASMA AND LIQUID PHASE SINTERED WC AND NbC BASED CEMENTED CARBIDE INSERTS

R.M. Genga^{1,2}, L.A. Cornish^{2,3}, M. Woydt⁴, K. Sobiya^{2,3} and C. Polese^{1,2}

¹School of Mechanical, Industrial and Aeronautical Engineering,
University of the Witwatersrand, South Africa

²DST-NRF Centre of Excellence in Strong Materials, University of the Witwatersrand,
South Africa

³School of Chemical and Metallurgical Engineering, University of the Witwatersrand,
South Africa

⁴BAM Federal Institute for Materials Research and Testing, Germany

Keywords: WC, NbC, SPS, Co, Fe₃Al, Hard-turning, Interrupted Milling, Flank Wear, Coolant-free, Crater Wear, Machinability

Abstract

The effects on the mechanical properties, thermal behaviour, response to cutting forces and wear mechanisms have been investigated for different manufacturing processes and materials for cemented carbide inserts. Spark plasma sintering (SPS) has been compared with liquid phase sintering (LPS), including NbC substitution for WC inserts, Ni and Fe₃Al substitution for the Co binder, and with Cr₃C₂, Mo₂C and TiC additions. The comparisons were conducted for coolant-free hard-turning and interrupted milling. Turning was carried out on 440B martensitic stainless steel (X90CrMoV18, 408 HV or 71.3 HRA) and interrupted milling was conducted on a structural steel (SABS 1431: 300WA, 184 HV or 55.1 HRA). The turning speed was varied from 80-120 m/min with a depth of cut between 0.5-1 mm, while the milling speed was varied from 100-250 m/min with a depth of cut of 1 mm. The cutting edge temperature (>1000 °C) was measured using a thermal camera (30 thermal readings per second) and force measurements were made by a Kistler dynamometer attached to the workpiece clamp. During turning, both SPS and LPS WC inserts had lower flank wear rate (FWR) values than the NbC inserts at all speeds. The LPS inserts had lower FWR values than the SPS inserts at low speeds, but the opposite occurred at high speeds. However, during milling, the NbC-12Co (ie NbC with 12 wt.%Co binder alloy) insert had a lower FWR than the SPS WC-10Co insert at 100 m/min and performed better than both the SPS and LPS WC-10Co at 250 m/min. Additions of TiC and Mo₂C to the WC inserts lowered FWR and improved the crater wear resistance in both turning and milling. No crater wear was observed in the NbC inserts due to its low solubility in the alloys. During hard turning, the NbC-12Co inserts performed better than the NbC-12Fe₃Al inserts. Wear was investigated by optical microscopy and high angle annular dark field scanning transmission electron microscopy (HAADF-STEM), and the results are explained by the composition and mechanical properties of the inserts.

Introduction

Tungsten carbide (WC) cemented carbides consist of a high volume fraction of hard ceramic (WC) within a tough metal binder matrix (Co, Ni or Fe) [1,2]. WC-based cemented carbides are commercially one of the oldest and most successful powder metallurgy products due to their good combination of hardness, toughness, strength, chemical stability and wear resistance [1-3]. Their unique combination of good physical, mechanical and chemical properties, as well as their proven service record in diverse applications over the past decades, have led to WC-based cemented carbides being the most well-used tool material today [4]. Approximately 70% of metal cutting tools (inserts) are made from WC cemented carbides; the remaining 30% comprises high speed steel (HSS), ceramics and TiC-based cemented carbides [4].

During metal cutting, the temperature at the insert/workpiece interface and chemical interaction at the insert/chip interface are the two main phenomena which affect the tool life [4,5]. Cutting temperatures around 1000 °C and above have been recorded during machining [4,6], reducing the hardness and strength of WC-based inserts, despite their good room temperature properties [1,4]. Interaction between the insert cutting edge and the workpiece, due to high contact pressure and cutting temperatures, leads to chemical adhesion and eventually tool wear by crater wear [1,4]. Crater wear results from the diffusion of atoms from the insert into the flowing nascent surfaces of chips from the workpiece, which are carried away from the insert/chip interface [5,7]. This material transport results in the formation of a “crater” on the rake face at a short distance from the cutting edge and, with continued machining, the crater increases in size and weakens the cutting edge, leading to failure [7]. Crater wear in WC-based inserts is mostly observed during machining of steel alloys, because of Fe’s higher affinity for C than W [1,8,9].

To improve the tool life of WC-Co-based inserts during machining of steels, better high temperature properties and chemical stability are required. Hot hardness and abrasion wear resistance can be increased by additions of VC, Cr₃C₂, TiC, TaC and Mo₂C [1,6,7,10]. Spark plasma sintering (SPS) significantly increases the hardness and abrasion wear resistance of WC cemented carbides compared to conventional liquid phase sintering (LPS) [6,11]. The technique employs high heating rates and high compressive pressure to consolidate powder compacts to a high density in a short time [12]. Its main advantage is the high degree of densification obtainable at low temperatures within a short period of time, compared to LPS [13]. The short sintering time does not allow for continuous Ostwald ripening, resulting in fine carbide grains and hence higher hardness [14]. Hot hardness, resistance to thermal cracking, abrasion wear resistance and corrosion resistance can also be increased by substitution of the Co binder with Ni [15]. Due to its more ductile austenitic structure, Ni reduces loss of WC grains by extruding outwards to replace the eroded binder between the WC grains, improving the wear resistance [16]. The chemical stability of WC-based inserts can be increased by additions of TiC and NbC [1]. Also, Ni has higher solubility and better wetting of TiC than Co [17], improving the resistance to diffusion wear, particularly for machining of steel [11]. Crater wear can also be prevented through complete substitution of WC by NbC, which has significantly lower solubility in steel [8,9]. NbC has good mechanical and physical properties, such as high hardness (19.6 GPa), very high melting point (3600 °C) (good for high temperature applications) and low density (7.89 g/cc) [1,9,14,18]. Intermetallic aluminides, such as iron aluminide, have also been studied as potential Co binder substitutes [19], because of their good strength at intermediate

temperatures and corrosion resistance at elevated temperatures [19]. Fe_3Al has no phase transitions over temperature and is composed of cheap elements. Use of iron aluminide (Fe_3Al) as a WC binder significantly improves the hardness, wear resistance, elastic modulus and corrosion resistance compared to Co [19]. However, Fe_3Al as a binder reduces the fracture toughness (K_{Ic}) and transverse rupture strength (TRS) of the WC cemented carbide compared to Co [19].

The effect of SPS, WC substitution with NbC, Co substitution with Ni and Fe_3Al , variation of binder content and TiC, Mo_2C , Cr_3C_2 additions on the mechanical properties and tool life of inserts under coolant-free, hard-turning and interrupted milling conditions, were investigated and compared to plain WC-10Co (wt.%) (ie WC with 10 wt.%Co binder alloy) inserts produced by SPS and LPS. The interest in NbC is because of its ready availability and its recently recognised intrinsic wear resistance [8].

Experimental Procedure

Materials

The starting powders and their characteristics are given in Table I. The powder compositions (Table II) were wet milled in 99% pure ethanol for 15 hours in a steel container with WC milling balls. They were then dried using a Rota evaporator at 64 °C at 80 rpm for 1 hour. The NbC grades were received from the University of Leuven (Katholieke Universiteit Leuven, Belgium).

Table I. Specifications of Starting Powders

Compound	D50 Particle size (μm)	Crystal Structure	Purity (wt.%)	Source
WC	0.8	hexagonal	>99.00	H.C. Starck, Germany
Co	0.9	hexagonal	>99.80	OMG Americas, USA
Ni	0.2	cubic	>99.80	Dong Yang (HK) International Group, China
Cr_3C_2	0.8	orthorhombic	>99.00	H.C. Starck, Germany
TiC	1.5	cubic	>99.00	Treibacher, Austria
NbC	1.2	cubic	>99.00	Treibacher, Austria
Mo_2C	1.7	orthorhombic	>99.00	Treibacher, Austria

Table II. Nominal Compositions of the Cemented Carbides (wt.%)

Abbreviation	Binder Phase			Alloying Additives				Hard Phase	
	Co	Ni	Fe ₃ Al	TiC	Mo ₂ C	Cr ₃ C ₂	Al ₂ O ₃	WC	NbC
WC-10Co	10	-	-	-	-	✓	-	Balance	-
WC-11Ni	-	11	-	✓	✓	✓	-	Balance	-
WC-7Ni	-	7	-	✓	✓	✓	-	Balance	-
NbC-12Co	12	-	-	-	-	-	-	-	Balance
NbC-12FA	-	-	12	-	-	-	✓	-	Balance

Sintering

The milled composite powders were consolidated in a spark plasma sintering furnace (HP D5, FCT Systeme, Germany). The powders were poured into cylindrical graphite dies with inner and outer diameters of 20.9 mm and 40 mm, respectively and 48 mm height. The composite powder assemblies were heated in a vacuum (2 Pa) in two steps, for example WC-10Co powders were first heated to 1000 °C at a rate of 200 °C/min and subsequently to 1220 °C at a heating rate of 100 °C/min, and the temperature was held at 1220 °C for five minutes during sintering. A cooling rate of 200 °C/min was applied to all samples. The applied pressure was adjusted from 16 MPa to 30 MPa at 1000 °C, and from 30 MPa to 50 MPa at 1220 °C within 30 seconds. The pressure was then held constant at 50 MPa throughout the rapid sintering cycle. Horizontal and vertical graphite papers were used to separate the powders from the die and punch setup. Hexagonal boron nitride was placed on the graphite paper to prevent C diffusion from the graphite paper to the powders during sintering. The graphite die was wrapped in a C cloth to minimize the heat loss from the die surface. The temperature was controlled by an optical pyrometer focused on a central borehole on the upper punch, 1 mm above the top surface of the sample, to give an accurate estimation of the sample temperature [14]. Consolidation of the composite powder assemblies in the axial direction was monitored by following the position of the plunger. Different sintering profiles, depending on the powder compositions, were used to achieve good densification, Table III.

Table III. Sintering Conditions

Composition (wt.%)	Abbreviation	Temperature and Dwell Time	Pressure (MPa)
WC-Cr ₃ C ₂ -10Co	10Co-S	1220 °C for 5 min	50
WC-Cr ₃ C ₂ -10Co	10Co-L	1430 °C for 75 min	4.4
WC-Cr ₃ C ₂ .Mo ₂ C-TiC-11Ni	11Ni-S	1320 °C for 5 min	70
WC-Cr ₃ C ₂ .Mo ₂ C-TiC-11Ni	11Ni-L	1430 °C for 75 min	4.4
WC-Cr ₃ C ₂ .Mo ₂ C-TiC-7Ni	7Ni-S	1380 °C for 5 min	70
WC-Cr ₃ C ₂ .Mo ₂ C-TiC-7Ni	7Ni-L	1430 °C for 75 min	4.4
NbC-12Co	NbC-12Co	1280 °C for 4 min	30
NbC-12Fe ₃ Al	NbC-12FA	1300 °C for 4 min	30

S = spark plasma sintered, L = liquid phase sintered

Liquid phase sintering (HIP, Ultra Temp, USA) was done by heating the compositions in a vacuum (0.04 MPa) at an initial heating rate of 2.4 °C/min up to 1200 °C. At 1200 °C, Co loss protection (CLP) was carried out by the addition of argon gas at a pressure of 0.37 MPa, and a heating rate 3.5 °C/min up to 1430 °C. The temperature was held constant for 75 minutes, and for the last 20 minutes, hot isostatic pressing (HIP) was done at 4.4 MPa to eliminate all the surface porosity [1]. The furnace was then water cooled at a rate of 3.5 °C/min.

Characterization and Mechanical Testing

Archimedes' principle was used to determine the density of the sintered samples (ED224S, Sartorius, Germany). Vickers hardness (HV 30) was measured on polished specimens after standard metallographic preparation, using a load of 30 N (VHT 003 MTA, Vickers Limited, United Kingdom), calculating an average from five indentations at different regions on each sample. The criteria for the accurate derivation of fracture toughness (K_{Ic}) using Shetty's equation were satisfied [20]: $1.25 \leq c/a \leq 2.25$ and $0.25 \leq I/a \leq 2.5$, where c is the Palmqvist crack length from the centre of indentation to the crack tip, a is half the diagonal length of indentation and I is the difference between c and a .

Turning trials were carried out on 440B martensitic stainless steel (440B-SS, X90CrMoV18), the chemical composition of this workpiece is shown in Table IV [21]. The 440B-SS has a Rockwell-A hardness of 71.31 ± 0.43 HRA. An EFAMATIC RS-20.2 CNC turning machine using an Oi-TD Fanuc series controller was used for the trials. The cutting tool inserts were secured on a CSBNL 3225P12 tool holder which matched the shape of the inserts. The inserts were square-shaped (12.7 x 12.7 x 4.3 mm), with a nose radius of 1.6 mm. All the inserts had a 0.2 mm land (chamfer) to reduce the stress concentration along the sharp cutting edges. The turning conditions are shown in Table V. The diameter of the workpiece was 50 mm and the length was 200 mm. The average tool wear was measured after each pass and the ISO 3685-1993 flank wear failure criterion was used [22,23]. According to this standard, a maximum flank wear of 300 μ m is acceptable, beyond which the insert can no longer achieve an acceptable surface finish [22].

During the coolant-free milling trials, the inserts were secured on to a Pilot F75SN12080 cutting tool holder attached to a Bridgeport GX1000 CNC milling machine with an Oi-MC Fanuc series controller. The milling trials were carried out on SABS 1431:300WA structural steel, of composition shown in Table IV [24]. The 300WA-SS had a hardness of 55.11 ± 0.65 HRA. The milling inserts had the same shape as the turning inserts. The milling conditions are shown in Table VI. The workpiece width was 60 mm and the radial depth of cut was 80 mm, ensuring that the inserts would disengage from the workpiece for rapid cooling every revolution. The flank wear was also measured after every pass and the ISO 3685-1993 flank wear failure criterion was used [23]. Maximum temperatures and thermal variation per second were measured using a thermal imaging camera (D5000, NIKON Japan), with Flir tool software; an example of a thermal image during turning is shown in Figure 1. The thermal camera took 30 thermal readings per second, facilitating measurement of the temperature change of the inserts. Force measurements were carried out using Kistler force gauges (9265, 3 axis dynamometer Kistler, Switzerland, for turning and 9366CC0, Kistler multicomponent force link, Switzerland, for milling). The Kistler force gauges were attached to the workpiece clamp.

The flank wear and crater wear were evaluated using an optical microscope (DM6000M, LEICA, Germany) with a digital camera (DFC490, LEICA, Germany) and high angle annular dark field scanning transmission electron microscopy (HAADF-STEM) (JEOL 2100, with a LaB₆ filament, JEOL, Japan).

Table IV. Chemical Compositions of the Workpiece Materials [21,24]

Workpiece Alloy	Constituent Elements (wt.%)									
	C	Si	Mn	V	Mo	Cr	P	S	Al	Fe
440B-SS	0.9	0.45	0.40	1.0	1.10	17.50	-	-	-	Balance
300WA-SS	0.18	0.34	1.35	-	-	-	0.02	0.03	0.04	Balance

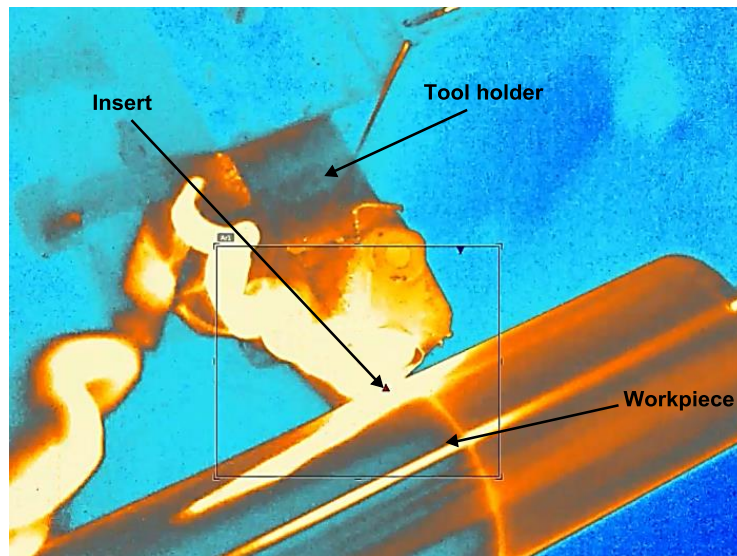


Figure 1. Thermal image during coolant-free turning.

Table V. Turning Conditions for the WC Cemented Carbide Inserts, a Feed Rate (V_f) of 0.1 mm/rev was used for all Cutting Tests

Cutting Speed, v_c (m/min)	Depth of Cut, a_p (mm)
80	1.0
100	1.0
120	0.5

Table VI. Milling Conditions for the WC Cemented Carbide Inserts, a Feed of 0.1 mm/tooth was Used for all Cutting Tests

Milling Test Variables		CNC Parameters	
Cutting speed, v_c (m/min)	Axial depth of cut, a_p (mm)	Spindle speed (rpm)	Feed rate (mm/min)
100	1.0	398.00	39.80
250	1.0	995.00	99.50
255	0.5	995.00	99.50

Results and Discussion

Densification

The NbC-based cemented carbides were produced by SPS, while the WC-based cemented carbides were produced by both SPS and LPS (Table III). All the sintered compositions achieved densifications above 99% and had negligible open porosity (Table VII), affirming the ability of SPS to produce dense compacts at much lower temperatures and shorter dwell times than LPS [12]. The WC-Ni samples required higher sintering temperatures (1320-1380 °C) and pressure than the WC-Co samples (1280 °C) to achieve good densification, yet they were all produced by SPS (Table VII). Sintering temperatures depend on several factors, such as diffusion rates, wetting of WC by the binder, solubility of WC in the binder, additives and binder proportion [1,11]. Therefore, the higher sintering temperatures can be attributed to the lower solubility of WC in Ni [10], the poorer wetting of WC by Ni [1,11] and the fact that the solubility of Mo₂C in Ni increases with increased sintering temperature [25]. The 7Ni-S sample was spark plasma sintered at a higher temperature (1380 °C) than the 11Ni-S sample (1320 °C), and this was attributed to the reduction in volume fraction of the lower melting point Ni binder [1,26].

The WC-10Co (wt.%) (10Co) sample required a lower SPS temperature than the NbC-12Co sample (Tables III and VII) to achieve good densification, because Co has much higher solubility and better wetting of WC than NbC [14]. The Fe₃Al binder, NbC-based sample (NbC-12FA) required a higher sintering temperature (T = 1300 °C, 30 MPa) than the NbC-12Co sample to achieve good densification (T = 1280 °C, 30 MPa), because of the better solubility between NbC and Co at temperatures above 1200 °C than in Fe₃Al [27].

Table VII. Density and Open Porosity of Sintered Samples

Abbreviation	Densification (%)	Volume open porosity (%)
10Co-S	99.75 ± 0.09	0.01 ± 0.00
10Co-L	99.85 ± 0.14	0.07 ± 0.01
11Ni-S	99.61 ± 0.24	0.02 ± 0.01
11Ni-L	99.75 ± 0.16	0.03 ± 0.02
7Ni-S	99.02 ± 0.20	0.04 ± 0.01
7Ni-L	99.76 ± 0.12	0.00 ± 0.00
NbC-12Co	99.20 ± 0.12	0.02 ± 0.01
NbC-12FA	99.27 ± 0.02	0.03 ± 0.01

S = spark plasma sintered, L = liquid phase sintered

Mechanical Properties

All the WC-based samples produced by SPS had higher Vickers hardnesses than the similar samples produced by LPS, Table VIII and Figure 2. This trend was confirmed by the Rockwell hardness tests, Table VIII. This was attributed to the lower sintering temperatures and shorter sintering dwell times which resulted in finer WC microstructures due to reduced Ostwald ripening [11,26]. Additions of TiC and Mo₂C to the WC-Ni cemented carbides produced by both LPS and SPS increased the hardness compared to WC-10Co, with the 7Ni-S grade having the highest hardness of >20 GPa, Table VIII. This increased hardness was due to TiC having higher hardness than WC by ~5 GPa [28]. Also, Ti is a good inhibitor for the growth or dissolution of WC by forming an atomic layer of TiC at the WC/Ni interface, altering the interfacial energy [6]. Mo₂C additions improved the hardness by improving the wetting of WC by Ni [1], leading to better binder distribution and higher hardness [1,14]. Furthermore, Mo₂C also acts as a WC grain growth inhibitor, refining the WC grain size by delaying the aggregation of fine WC and the transformation of the aggregates to single large grains (coalescence) during sintering [26,29]. Both the NbC-based samples had lower hardnesses than the WC-based samples, because NbC has a lower hardness (~19.4 GPa) than WC (~22.5 GPa) [30]. The lower hardnesses could also result from the lower solubility and poorer wetting of NbC by Co and Fe₃Al [14,27]. The NbC-12FA sample had a slightly higher hardness than the NbC-12Co sample, most likely due to the intermetallic Fe₃Al having a higher hardness than Co [19]. However, for cutting tool applications, inserts with similar hardnesses are normally compared.

The WC-10Co samples produced by SPS and LPS had the highest fracture toughnesses (K_{Ic}) compared to the WC-Ni-based samples, because of the good wetting of WC by Co compared to Ni, improving the Co binder distribution [6,11,26]. Liquid phase sintered WC-10Co had a higher K_{Ic} than the similar sample produced by SPS, and this trend was also observed in the WC-Ni-based samples. The higher K_{Ic} was due to better binder pool distribution from the formation of the Co-liquid phase during sintering [11,26] which enhanced WC solubility [1], as well as the capillarity action of the liquid phase between the pores during the secondary rearrangement stage of sintering [1]. However, during SPS, the liquid binder phase only exists momentarily, followed by rapid solidification [11,12], preventing enhanced WC solubility and secondary rearrangement due to capillary action of the liquid phase, resulting in poorer binder distribution. The 11Ni-L sample had a higher K_{Ic} than the 7Ni-L sample, due to the higher volume fraction of the tougher

binder phase [1]. The tougher metallic binder phase shields the stress field at the front of the crack tip during crack propagation and bridges the crack ligaments behind the crack tip [31]. The NbC-12Co sample had a much lower K_{Ic} value than all the 10Co-S samples, although with a higher Co binder amount. This was attributed to the poorer solubility and wetting of Co with NbC than with WC [14], leading to formation of brittle interconnected NbC networks, due to poorer distribution of Co [31]. The NbC-12FA sample had a lower K_{Ic} than NbC-12Co, due to the even poorer solubility and wetting of the Fe_3Al with NbC than Co [27], as well as the lower ductility of Fe_3Al than Co [19].

Table VIII. Mechanical Properties of the Samples

Abbreviation	Vickers Hardness, HV 30 (GPa)	Rockwell-A Hardness, HRA (60 kgf)	Fracture Toughness, K_{Ic} (MPa.m ^{1/2})
10Co-S	17.34 ± 0.10	93.02 ± 0.13	11.84 ± 0.16
10Co-L	15.03 ± 0.13	90.20 ± 0.18	12.71 ± 0.23
NbC-12Co	12.86 ± 0.14	89.86 ± 0.11	7.87 ± 0.18
NbC-12FA	13.21 ± 0.11	89.86 ± 0.28	6.65 ± 0.19
7Ni-S	20.36 ± 0.11	94.60 ± 0.35	10.18 ± 0.15
7Ni-L	18.00 ± 0.27	93.48 ± 0.12	10.69 ± 0.23
11Ni-S	18.85 ± 0.19	93.58 ± 0.24	10.38 ± 0.43
11Ni-L	15.96 ± 0.15	92.02 ± 0.27	11.22 ± 0.16

S = spark plasma sintered, L = liquid phase sintered

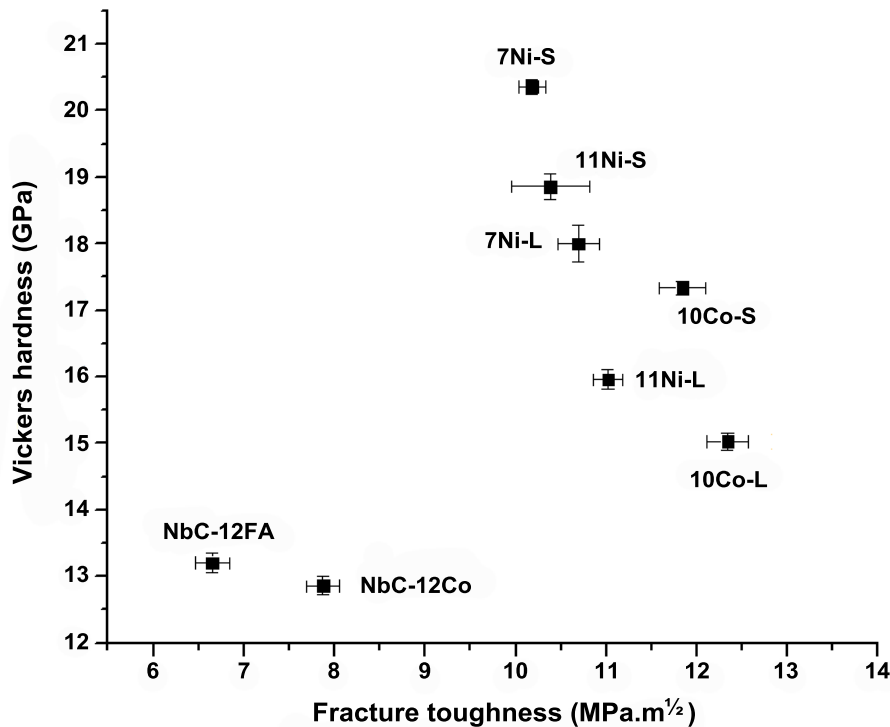


Figure 2. Relationship between Vickers hardness and Palmqvist fracture toughness.

Flank and Crater Wear During Hard-turning

The flank wear rate (FWR), average resultant force (F_R) and temperature measurements during turning at a cutting speed (v_c) of 80 m/min and a depth of cut (a_p) of 1 mm are shown in Table IX. The 7Ni-L insert had the lowest FWR followed by the 10Co-S insert, while the NbC-12Co insert had the highest FWR, Figure 3, although all the inserts experienced similar average temperatures and maximum recorded temperatures of above 1380 °C, Table IX. The high maximum temperature recorded gives an indication of the aggressive cutting conditions the inserts were exposed to during hard turning of 440B martensitic steel.

Generally, insert failure during machining can be attributed to two main causes: chemical wear (diffusion) and mechanical wear (abrasion, attrition and fracture) [5,21]. Compared to WC, NbC is chemically more stable, forms Nb_2O_5 (a non-volatile reaction layer) and has better higher temperature properties than WC, especially during machining of steels [8,9]. However, the NbC insert had the highest FWR compared to all the WC-based inserts, which was attributed to mechanical wear [5]. Flank wear is mainly caused by rubbing at the insert cutting edge/nascent workpiece interface, resulting in abrasive and/or adhesive wear at high temperatures [5]. Abrasion is the main flank wear mechanism and is characterised by formation of grooves, Figure 3, in the direction which the insert slides against the workpiece surface [5]. The flank wear was mainly due to mechanical wear attributed to the high hardness of the 440B-SS workpiece (71.31 ± 0.43 HRA) which acted as an abrasive body. Additionally, the debris from the workpiece that normally gets trapped at the cutting edge/workpiece interface during turning would undergo plastic deformation and strain hardening, forming hard abrasive bodies [32], increasing the flank wear [5]. The higher flank wear in the NbC-12Co sample than the WC-based inserts could also be due to mechanical wear from vibration of the workpiece at the low turning speed of 80 m/min [33], which led to high cutting forces, Table IX. The average cutting forces at 80 m/min were much higher than at 100 m/min, although the same depth of cut (1 mm) was used, Figure 4, and that was attributed to reduced vibration at the higher cutting speed [33]. The NbC-12Co insert had a lower K_{Ic} , Table VIII, and lower TRS than the LPS inserts [6,34,35], lowering the resistance to the cyclic impact force introduced by the vibrations at 80 m/min, leading to higher flank wear, but did not show any flaking like the 10Co-S sample, Figure 3. The NbC-12FA insert shattered at a $v_c = 80$ m/min and $a_p = 1$ mm during turning because of its even lower K_{Ic} and TRS than all the other inserts, leading to some fracture of NbC grains along the cutting edge, Figure 5. It has to be noted that the 7Ni-S also shattered under these conditions, Table IX.

All the inserts produced by LPS had better FWR than similar compositions produced by SPS during turning at 80 m/min, which could be due to their higher K_{Ic} and TRS values. The lower TRS in the SPS samples was also due to higher residual stresses from the rapid cooling rates compared to LPS [6,34], explaining why only SPS inserts shattered during turning. Generally, the average F_R increased with increased FWR, due to flank wear leading to blunting of the cutting edge, which increased the cutting force because of increased shear area [36]. Cutting force increases with increased shear force, and the shear force increases with increased shear area [36]. Crater wear was observed on the rake of the 10Co-S insert, but not on any of the Ni-bonded WC inserts, Figure 3. The main mechanism during crater wear was diffusion of WC from the insert cutting edge into the workpiece, leading to dissolution of the insert surface by the chips

flowing over it, which was activated by high cutting temperature [1,5]. Crater wear occurred on 10Co-S due to the diffusion of W and C (mainly C) into the steel due to good chemical affinity, particularly above 1200 °C [1,8]. Additions of TiC and Mo₂C to WC-based cemented carbides improve the resistance to crater wear by forming the (W,Ti,Mo)C solid solution which has very good chemical stability at high temperatures [1], explaining the resistance to crater wear in the 7Ni and 11Ni inserts. No crater wear was observed in any of the NbC inserts, Figure 3, because NbC is chemically stable at high temperatures and is nearly insoluble in Fe above 1200 °C [8,9].

Table IX. Comparison of Insert Behaviour During Coolant-free Turning
at a $v_c = 80$ m/min and $a_p = 1$ mm

Insert	Flank Wear Rate, FWR ($\mu\text{m}/\text{min}$)	Average Resultant Force, F_R (N)	Average Cutting Temperature ($^{\circ}\text{C}$)	Maximum Recorded Temperature ($^{\circ}\text{C}$)
10Co-S	15.65	1054.42 ± 19.76	1117 ± 201	1435
NbC-12Co	40.16	1079.81 ± 20.67	1067 ± 137	1380
NbC-12FA	Shattered	-	-	-
7Ni-S	20.26	1031.65 ± 30.43	1044 ± 185	1418
7Ni-L	13.38	960.19 ± 16.82	1110 ± 214	1489
11Ni-S	Shattered	-	-	-
11Ni-L	18.87	963.89 ± 23.46	1018 ± 216	1457

S = spark plasma sintered, L = liquid phase sintered

The FWR and average F_R of the inserts due to turning at $v_c = 100$ m/min and $a_p = 1$ mm are shown in Table X. There were lower cutting forces at 100 m/min than at 80 m/min, which was attributed to the reduced vibration on the workpiece at the higher cutting speed [33]. The LPS inserts had lower FWR than the SPS inserts, with 11Ni-L having the lowest FWR and NbC-12FA having the highest FWR. The aggressive nature of hard-turning meant that mechanical wear could be the major cause of flank wear at 100 m/min, hence the lower TRS and K_{ic} of the SPS inserts than the LPS inserts explains the higher FWR of the SPS inserts [6], as well as the shattering of the 7Ni-S insert. The NbC-12Co insert had a slightly lower FWR than the 10Co-S insert, Table X and Figure 6, which could be due to the lower average F_R (reduced workpiece vibration, eliminating the effect of cyclic impact at the cutting edge), and the better high temperature properties of NbC than WC [8,9]. The NbC-12FA insert had the highest FWR and highest average F_R , and the latter was because of blunting of the cutting edge, which increased with increased flank wear [6,36].

Lower average resultant forces were observed while turning at $v_c = 120$ m/min and $a_p = 0.5$ mm than at the lower cutting speeds, Table X, due to the reduced a_p [6]. Similar to the previous trends, the WC-Ni-based inserts had lower FWR than the 10Co-S and NbC-12Co inserts, with 7Ni-S having the lowest FWR, Table X. Abrasion and adhesion are key mechanical wear mechanisms at high cutting speeds [5], and are dependent on the hardness and bonding strength of the material (inserts) [1,5,6], and usually materials with similar hardnesses are compared. Additions of TiC and Mo₂C improve the high temperature hardness [1], increasing the resistance to abrasion, while Mo₂C improves the bonding between WC and Ni [11], thus increasing

resistance to adhesion [5]. Consequently the 10Co-S insert had a lower abrasion wear resistance than the WC-Ni inserts [6] and lower resistance to deformation at high temperature due to the absence of TiC and Mo₂C, increasing its FWR at 120 m/min [6].

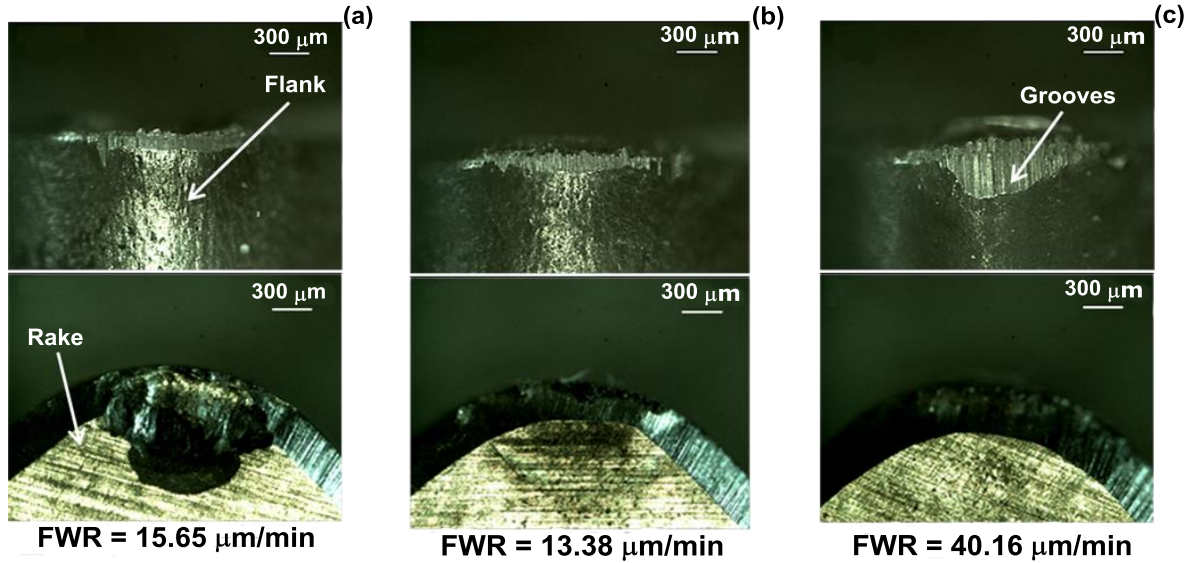


Figure 3. Wear on the flank and rake of; (a) 10Co-S, (b) 7Ni-L, (c) NbC-12Co cutting tool inserts from coolant-free turning at a $v_c = 80$ m/min and $a_p = 1$ mm.

NbC has a low solubility in Fe, Ni, or Co at 1250 °C [27] and can, therefore, form a brittle NbC interconnected network with poor binder distribution [31]. The present NbC grades have regions without binder material and thus regions without any toughness provided by the binder.

Table X. Comparison of Insert Behaviour during Coolant-free Turning $v_c = 100$ and 120 m/min

Insert	$v_c = 100$ m/min, $a_p = 1$ mm		$v_c = 120$ m/min, $a_p = 0.5$ mm	
	FWR ($\mu\text{m}/\text{min}$)	Average Resultant, F_R (N)	FWR ($\mu\text{m}/\text{min}$)	Average Resultant, F_R (N)
10Co-S	30.44	726.69 ± 15.67	132.09	497.91 ± 16.67
NbC-12Co	26.12	639.52 ± 19.44	288.73	512.45 ± 26.44
NbC-12FA	40.32	780.80 ± 11.93	-	-
7Ni-S	Shattered	-	101.32	536.90 ± 37.13
7Ni-L	20.99	748.89 ± 10.64	62.93	517.41 ± 20.64
11Ni-S	22.77	734.89 ± 16.37	66.06	501.21 ± 15.83
11Ni-L	18.33	650.11 ± 23.38	72.14	531.21 ± 26.61

S = spark plasma sintered, L = liquid phase sintered

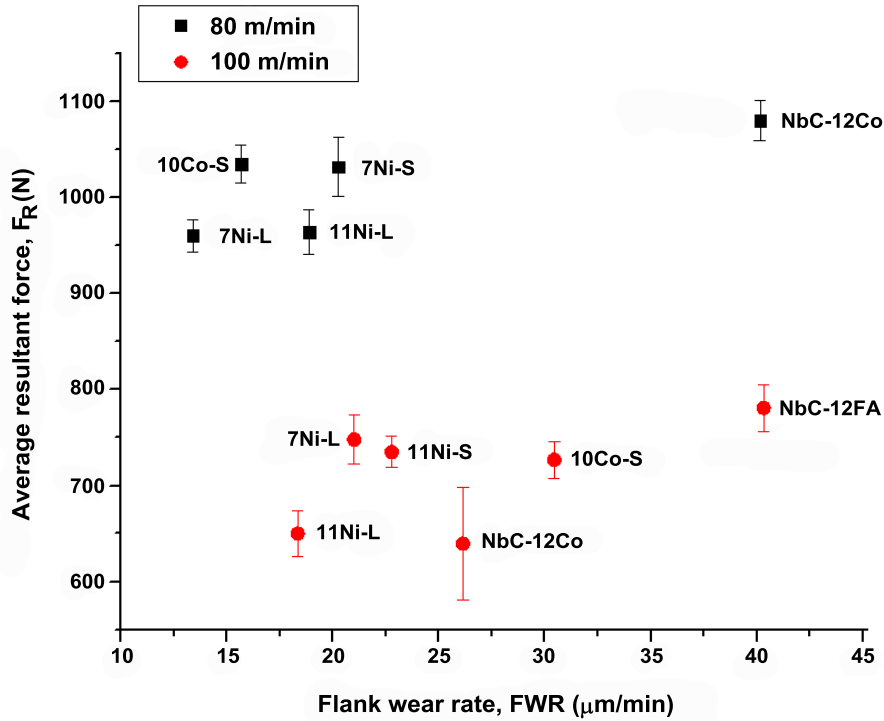


Figure 4. Comparison between average resultant force and FWR at $v_c = 80$ and 100 m/min and $a_p = 1$ mm during coolant-free turning.

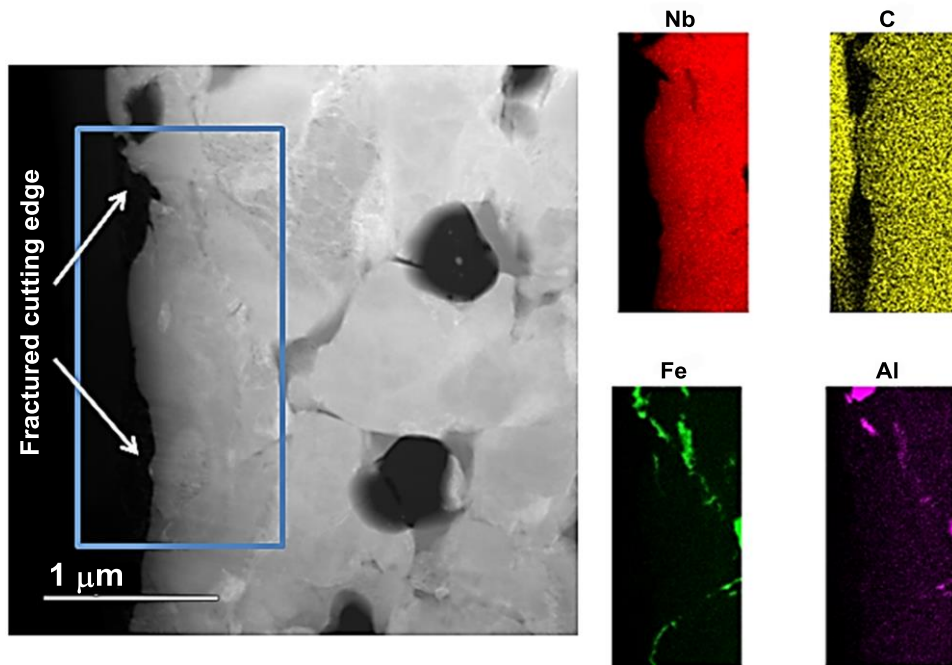


Figure 5. HAADF-STEM mapping images of the fracture cutting edge of the NbC-12Fe₃Al (wt.%) from coolant-free turning, showing Nb (red), C (yellow), Fe (green) and Al (purple).

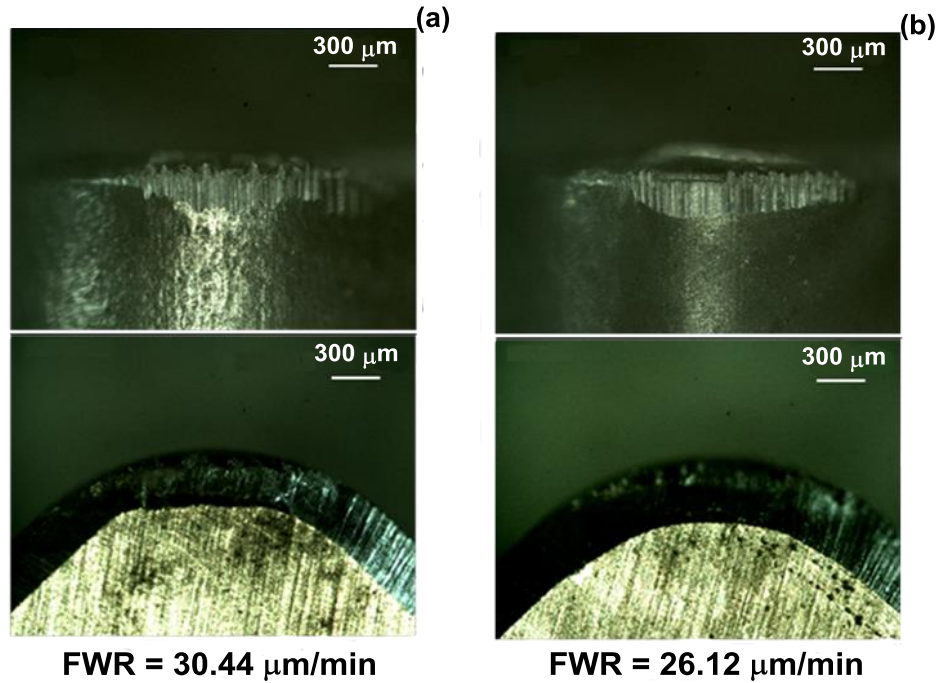


Figure 6. Flank wear on; (a) 10Co-S, (b) NbC-12Co cutting tool inserts from coolant-free turning at a $v_c = 100$ m/min and $a_p = 1$ mm.

The cyclic impact and rapid changes in temperature per revolution led to both mechanical wear from the cyclic impact and thermal shock [6], as well as chemical wear from the chemical affinity between the inserts and the 330WA-SS workpiece [1,5,6]. The inserts produced by LPS had lower FWR values because of the better thermal shock and impact resistances than inserts produced by SPS [6]. The good thermal shock and impact resistance were associated with higher TRS and K_{Ic} of the LPS inserts than the SPS inserts [6,35]. The 10Co-L insert had a higher FWR than the other liquid phase sintered inserts, and similarly, the 10Co-S had a higher FWR than the other spark plasma sintered inserts, Table XI.

Table XI. Comparison of Insert Behaviour during Coolant-free Milling at $v_c = 100$ m/min and $a_p = 1$ mm

Insert	Flank Wear Rate, FWR ($\mu\text{m}/\text{min}$)	Average Resultant Force, F_R (N)	Average Temperature Variation per Second, $\Delta T/s$ ($^{\circ}\text{C}/\text{second}$)
10Co-S	79.92	390.73 ± 47.41	440.70 ± 31.85
10Co-L	35.86	285.77 ± 32.28	384.75 ± 25.70
NbC-12Co	39.14	312.74 ± 34.63	393.34 ± 15.15
7Ni-S	70.44	352.25 ± 37.79	405.54 ± 24.24
7Ni-L	37.23	258.64 ± 30.17	388.71 ± 24.61
11Ni-S	44.91	376.68 ± 36.83	369.79 ± 10.96
11Ni-L	10.36	246.17 ± 27.58	370.71 ± 20.74

S = spark plasma sintered, L = liquid phase sintered

The higher FWR in the 10Co-S insert than the other SPS inserts was attributed to chemical wear and was confirmed by crater wear on the rake face of 10Co-S, Figure 7 [1]. The additions of TiC and Mo₂C improved the resistance to chemical wear in the 7Ni and 11Ni inserts. No crater wear and little flank wear were observed in the Nb-12Co insert, Figure 7, because of the good chemical stability of NbC [8,9]. The average F_R increased with increased FWR, Figure 8, which was attributed to blunting of the cutting edge [36]. The average temperature variation per second ($\Delta T/s$) also increased with increased FWR, due to blunting of the cutting edge which increased the friction at the cutting edge/workpiece interface [6]. Increasing v_c from 100 m/min to 250 m/min, while maintaining the same a_p (1 mm) resulted in both increased FWR and average F_R , Table XII. The increase in FWR was due to increased impact (increased number of collisions with workpiece per second), increasing the average F_R , as a result of increased blunting of the cutting edge [6]. Mostly, the $\Delta T/s$ reduced with increased v_c , because of the reduced cooling time per revolution (time between the insert disengagement with the workpiece and re-engagement with the workpiece in one revolution) due to increased spindle speed. This leads to increased minimum temperatures per revolution and hence reduced difference between the maximum and minimum temperature per second. The inserts produced by SPS had higher FWR than the similar ones produced by LPS, with 10Co-S having the highest FWR. The NbC-12Co insert had a significantly lower FWR than both 10Co-S and 10Co-L, Table XII and Figure 9, because of its better high temperature properties and higher resistance to chemical wear [8,9].

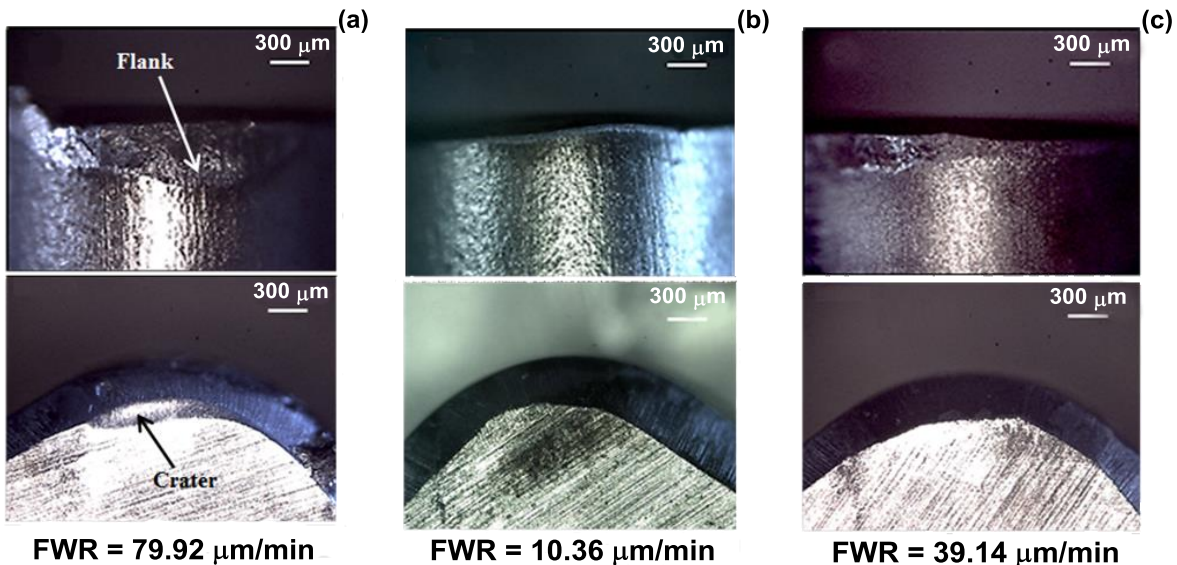


Figure 7. Wear on the flank and rake of; (a) 10Co-S, (b) 11Ni-L, (c) NbC-12Co cutting tool inserts from coolant-free milling at $v_c = 100$ m/min and $a_p = 1$ mm.

Crater wear was observed on the rake face of 10Co-L and was confirmed by HAADF-STEM mapping images of the rake face, Figure 10 which revealed a curved interface with smoothly worn WC grains, indicating diffusion between the insert and the workpiece [37]. However, HAADF-STEM mapping images of the rake face of the NbC-12Co insert revealed a straight interface, Figure 11, demonstrating the good chemical stability of NbC during machining of the steels [8,9]. Notching was observed on the flank of NbC-12Co, Figure 9, which was due to increased mechanical impact with increased v_c [6] and the lower K_{Ic} of the NbC cermets than the other inserts, Table VIII.

Table XII. Comparison of Insert Behaviour during Coolant-free Milling
at $v_c = 250$ m/min and $a_p = 1$ mm

Insert	Flank Wear Rate, FWR ($\mu\text{m}/\text{min}$)	Average Resultant Force, F_R (N)	Average Temperature Variation per Second, $\Delta T/s$ ($^\circ\text{C}/\text{second}$)
10Co-S	300.57	541.22 ± 46.41	365.48 ± 38.95
10Co-L	237.15	330.91 ± 39.05	369.60 ± 18.42
NbC-12Co	75.83	324.00 ± 24.61	331.51 ± 19.57
7Ni-S	74.65	383.49 ± 26.83	318.26 ± 38.94
7Ni-L	49.63	274.56 ± 35.49	271.21 ± 36.42
11Ni-S	142.01	408.05 ± 42.18	386.24 ± 21.11
11Ni-L	38.60	259.22 ± 22.05	296.87 ± 26.17

S = spark plasma sintered, L = liquid phase sintered

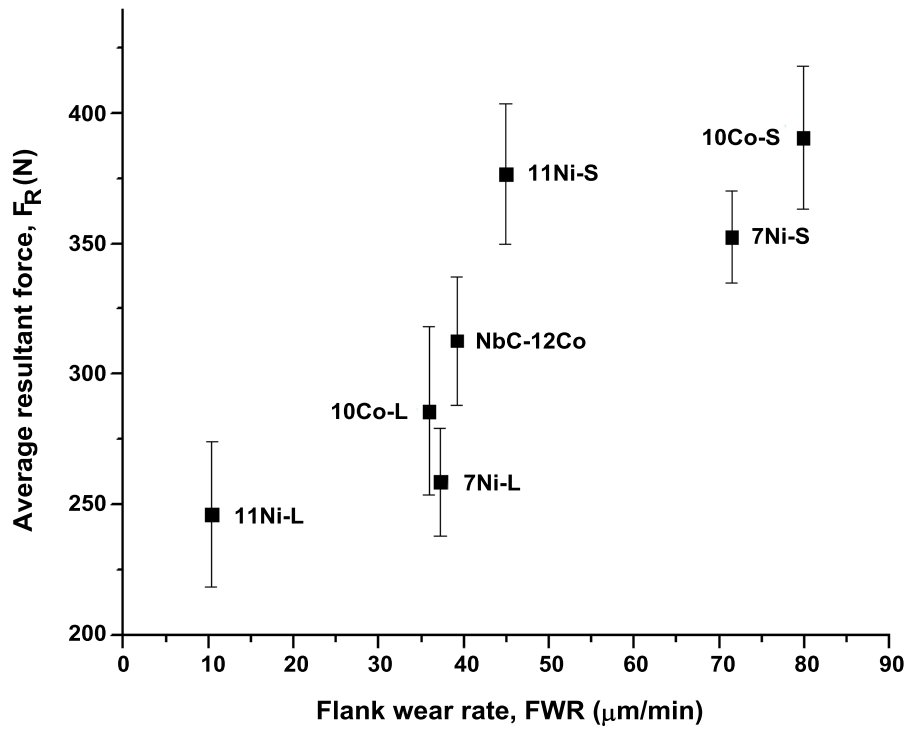


Figure 8. Comparison between average resultant force and FWR at $v_c = 100$ m/min and $a_p = 1$ mm during coolant-free milling.

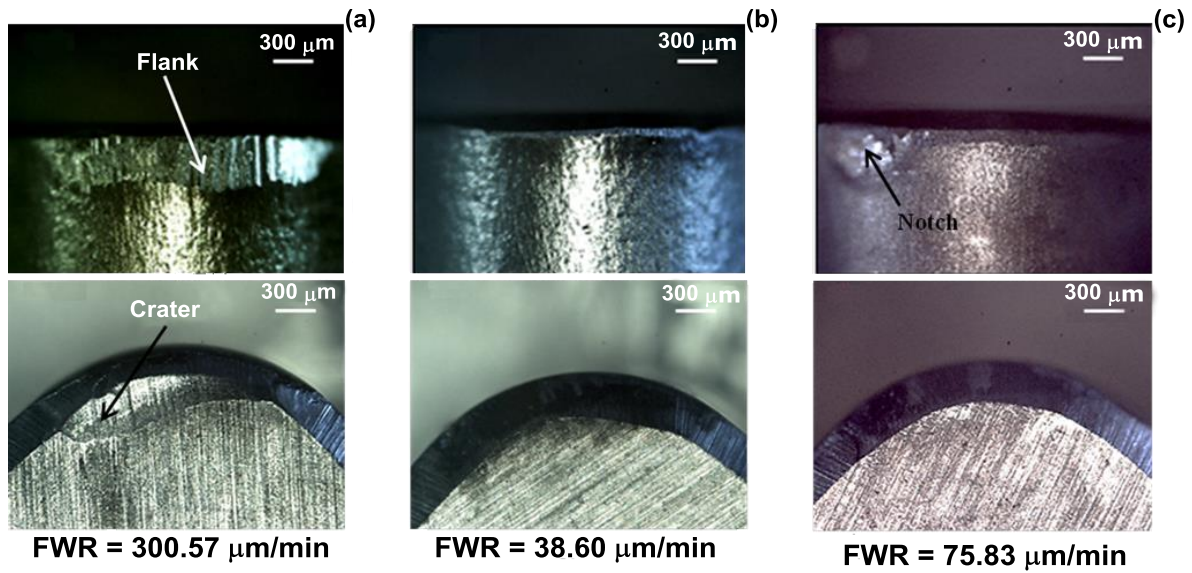


Figure 9. Wear on the flank and rake of; (a) 10Co-L, (b) 11Ni-L, (c) NbC-12Co cutting tool inserts from coolant-free milling at $v_c = 250$ m/min and $a_p = 1$ mm.

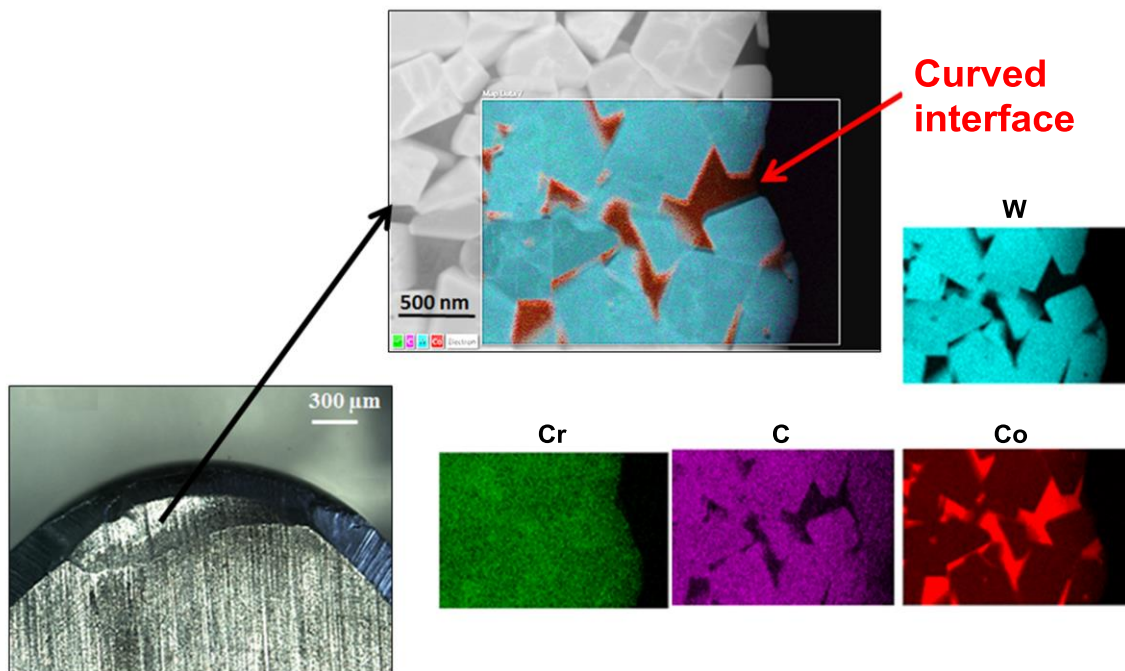


Figure 10. HAADF-STEM mapping images of the crater on the rake face under coolant-free milling of WC-10Co (wt.%), showing W (blue), Cr (green), C (purple) and Co (red).

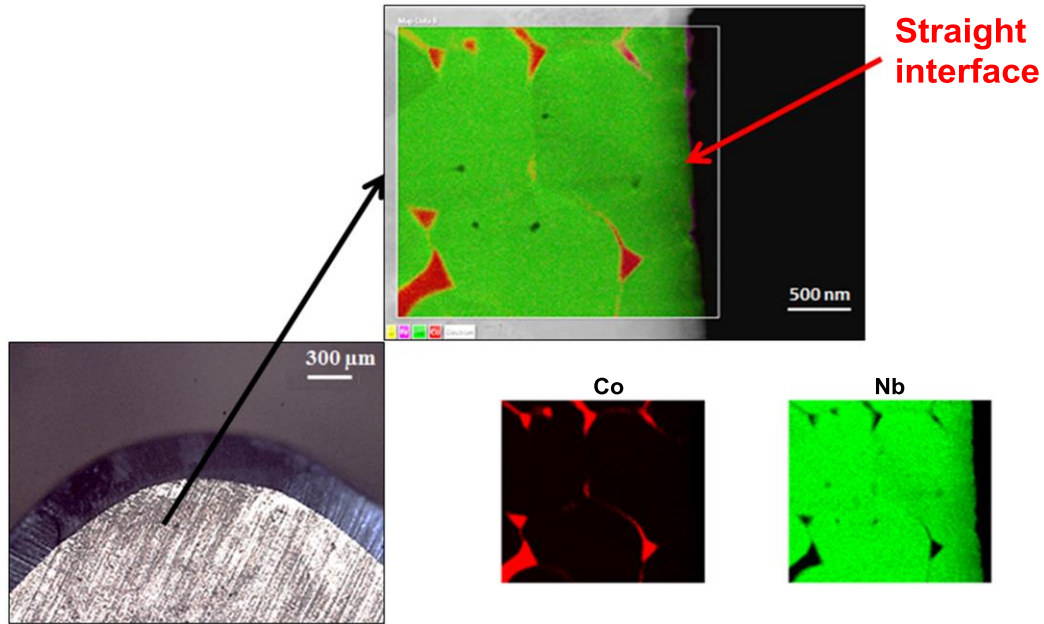


Figure 11. HAADF-STEM mapping images of the rake face under coolant-free milling of NbC-12Co, showing Co (red) and Nb (green).

Conclusions

1. Spark plasma sintering and liquid phase sintering were used to consolidate the WC- and NbC-based cemented carbides, producing inserts with good densification (above 99%) and negligible open porosity. The inserts produced by SPS had significantly higher hardness and lower K_{Ic} than similar LPS samples.
2. During hard-turning at 80 and 100 m/min, the inserts produced by LPS had lower FWR values than similar inserts produced by SPS, which were attributed to their better resistance to mechanical wear due to higher K_{Ic} and TRS.
3. Higher cutting forces were observed at 80 m/min than at 100 m/min, although the same a_p (1 mm) was used, which was attributed to vibration of the workpiece. The 7Ni-S insert had the lowest FWR at 120 m/min and a_p of 0.5 mm, due to its high hardness which improved its abrasion wear resistance.
4. The NbC-12Co inserts had a lower FWR than the 10Co-S at 100 m/min because of the reduced mechanical wear (reduced vibration effect) and better resistance to chemical wear, although during machining tests, inserts with similar hardnesses are normally compared.
5. Crater wear was observed in the 10Co-S insert, but not in the WC-Ni-based inserts, because of TiC and Mo₂C additions. No crater wear was observed in either NbC-12Co or NbC-12FA inserts, because of the good chemical stability of NbC and its low solubility in the machined steels.

6. During interrupted milling, inserts produced by LPS performed better than those produced by SPS for all cutting speeds, due to lower thermal shock resistance and lower impact resistance of the SPS.
7. Crater wear was also observed in the 10Co-S and 10Co-L inserts. No crater wear was observed on the WC-Ni grades and NbC-12Co inserts during milling. The NbC-12Co insert performed better than the standard WC-10Co grades at all milling speeds, showing potential as a possible replacement for WC-Co-based inserts for milling of steels. The 7Ni-L and 11Ni-L performed the best in all hard-turning and interrupted milling tests.

Acknowledgments

This work was financially supported by Department of Science and Technology and the National Research Foundation, South Africa. The authors are grateful to Pilot Tools (Pty) Ltd for assisting in the production of the cutting tools, Department of Mechanical Engineering Science at the University of Johannesburg for use of their turning machine, Professor Rolf Laubscher and Mr. Gerrard Peters for discussions and advice. The authors are grateful to Companhia Brasileira de Metalurgia e Mineração (CBMM), São Paulo, Brazil, for supplying the NbC grades.

References

1. G.S. Upahyaya, *Cemented Tungsten Carbide Production, Properties and Testing* (New Jersey, USA: Westwood, 1998), 55-301.
2. Z. Yao, J.J. Stiglich and T.S. Sudarshan, *Nano-Grained Tungsten Carbide-Cobalt (WC/Co)* (Virginia, USA: Material Modification, Inc, 1999).
3. K. Bonny et al., "Dry Reciprocating Sliding Friction and Wear Response of WC-Ni Cemented Carbides," *Tribology Letters*, 31 (2008), 199-109.
4. V.K. Sarin et al., *Comprehensive Hard Materials* (Oxford, UK: Elsevier, 2014).
5. S.A. Kumar, A.R. Durai and T. Sornakumar, "The Effect of Tool Wear on Tool Life of Alumina-based Ceramic Cutting Tools while Machining Hardened Martensitic Stainless Steel," *Journal of Materials Processing Technology*, 173 (2006), 151-156.
6. R.M. Genga et al., "Abrasion Wear, Thermal Shock and Impact Resistance of WC-Cemented Carbides Produced by PECS and LPS," *International Journal of Refractory Metals and Hard Materials*, 49 (2015), 133-142.
7. J. Hua and R. Shivpuri, "A Cobalt Diffusion Based Model for Predicting Crater Wear of Carbide Tools in Machining Titanium Alloys," *ASME*, 127 (2005), 136-144.
8. M. Woydt and H. Mohrbacher, "The Tribological and Mechanical Properties of Niobium Carbide (NbC) Bonded With Cobalt or Fe₃Al," *Wear*, 321 (2014), 1-7.

9. S.G. Huang et al., "VC and Cr₃C₂ Doped WC-NbC-Co Hardmetals," *Journal of Alloys and Compounds*, 488 (2008), 205-211.
10. N. Lin et al., "Effect of Mo and Co Additions on the Microstructure and Properties of WC-TiC-Ni Cemented Carbides," *International Journal of Refractory Metals and Hard Materials*, 30 (2012), 107-113.
11. R.M. Genga, L.A. Cornish and G. Akdogan, "Effect of Mo₂C Addition on the Properties of SPS Manufactured WC-TiC-Ni Cemented Carbide," *International Journal of Refractory Metals and Hard Materials*, 41 (2013), 12-21.
12. M. Tokita, *Mechanism of Spark Plasma Sintering*, (Kawasaki-shi Kanagawa, Japan: Sumitomo Coal Mining Company Ltd., 1999), 3-7.
13. X. Song, X. Liu and J. Zhang, "Neck Formation and Self Adjusting Mechanism of Neck Growth of Conducting in Spark Plasma Sintering," *Journal of the American Ceramic Society*, 89 (2006), 494-500.
14. S.G. Huang et al., "NbC as Grain Growth Inhibitor and Carbide in WC-Co Hardmetals," *International Journal of Refractory Metals and Hard Materials*, 26 (2008), 389-95.
15. A.M. Human and H.E. Exner, "Electrochemical Behaviour of Tungsten-Carbide Hardmetals," *Materials Science and Engineering*, 209 (1996), 180-191.
16. B. Wittmann, W.D. Schubert and B. Lux, "WC Grain Growth and Grain Growth Inhibition in Nickel and Iron Binder Hardmetals," *International Journal of Refractory Metals and Hard Materials*, 20 (2002), 51-60.
17. S.K. Bhaumik, S.G. Upadhyaya and M.L. Viadya, "Design of WC-Co Hard Metals with Modifications in Carbide and Binder Phases," *International Journal of Refractory Metals and Hard Materials*, 11 (1992), 9-22.
18. S.G. Huang, O. Van der Biest and J. Vleugles, "VC Doped WC-NbC-Co Hardmetals." *Materials Science and Engineering*, 488 (2008), 420-427.
19. S.G. Huang, O. Van der Biest and J. Vleugles, "Pulse Electric Current Sintered Fe₃Al Bonded WC Composites," *International Journal of Refractory Metals and Hard. Materials*, 27 (2009), 1019-1023.
20. D.K. Shetty et al., "Indentation Fracture of WC-Co Cermets," *Journal of Materials Science*, 20 (1985), 1873-1882.
21. K. Sodiya et al., "Performance of Mixed Ceramics and CBN During Hard Turning of Martensitic Stainless Steel," *International Journal of Advanced Manufacturing Technology*, 77 (2015), 861-871.

22. ISO 3685:1993, Tool-Life Testing with Single-Point Turning Tools (International Organization for Standardization, Geneva, 1993).
- 23 W.A. Knight and G. Boothroyd, *Fundamentals of Machining and Machine Tools, 3rd Edition* (Florida, USA: Taylor and Francis Group, LLC, 2006).
24. SABS 1431:1987 South Africa Bureau of Standards for Structural Steels.
25. P.M. Kemp and R.M. German, "Grain Growth in Liquid Phase Sintered W-Mo-Ni-Fe Alloys," *Journal of the Less Common Metals*, 175 (1991), 353-68.
26. R.M. Genga, L.A. Cornish and G. Akdogan, "Optimization of WC Particle Size, Ni Binder Content and Mo₂C Addition for Improved SPS WC-TiC-Ni Cemented Carbide" (Paper presented at the 18th Plansee Seminar, Reutte, Austria, 4 June 2013), 26.
27. R. Edwards and T. Raine, "The Solid Solubility of Some Stable Carbides in Cobalt Nickel and Iron at 1250 °C," *Powder Metallurgy, Springer-Verlag*, (1952), 232-242.
28. H.C. Kim, D.K. Kim and I.J. Shon, "Sintering Behaviour and Mechanical Properties of Binderless WC-TiC Produced by Pulse Current Activated Sintering," *Journal of Ceramic Processing Research*, 8 (2007), 91-97.
29. X. Wang, Z.Z. Fang and H.Y. Sohn, "Grain Growth during the Early Stage Sintering of Nanosized WC-Co Powders," *International Journal of Refractory Metals and Hard Materials*, 26 (2008), 232-42.
30. R.M. Genga et al., "Microstructure and Material Properties of PECS Manufactured WC-NbC-Co and WC-TiC-Ni Cemented Carbides," *International Journal of Refractory Metals and Hard Materials*, 49 (2015), 240-248.
31. S.G. Huang et al., "Properties of NbC-Co Cermets Obtained by Spark Plasma Sintering," *Materials Letters*, 61 (2007), 574-577.
32. B. Basu and M. Kalin, *Tribology of Ceramics and Composites: A Material Science Perspective* (New Jersey, USA: John Wiley & Sons, Inc., 2011), 51-54.
33. V.B. Gaba, J. Nookala and S.G. Babu, "The Impact of Cutting Conditions on Cutting Force and Chatter Length for Steel and Aluminium," *International Journal of Engineering and Advanced Technology*, 2 (2013), 919-924.
34. F. Zhang et al., "Spark Plasma Sintering of Macroporous Calcium Phosphate Scaffolds from Nanocrystalline Powders," *Journal of the European Ceramic Society*, 28 (2008), 539-545.
35. J. Gurland and P. Bradzil, "Relation of Strength, Composition and Grain Size of Sintered WC-Co," *Transactions of the Metallurgical Society of AIME*, 203 (1955), 311-315.

36. F.E. Gorczyca, *Application of Metal Cutting Theory* (New York, NY, USA: Industrial Press, 1987), 144-153.

37. E.M. Trent, *Metal Cutting, 4th Edition* (London, UK: Butterworth-Heinemann, 1991) 188-195.